Article ID: 1000-9116(2005)04-0410-09

Arrival time measurements of first arrival phases P and PKIKP using the method of fixed scale wavelet transformation ratio*

HE Xiao-bo (何小波) ZHOU Hui-lan (周蕙兰)
Computational Geodynamics Laboratory, *Graduate School of Chinese Academy of Sciences*, *Beijing* 100049, *China*

Abstract

The arrival times of first teleseismic phases are difficult to be measured precisely because of slowly and gradually changed onsets and weak amplitudes. The arrival times measured manually are usually behind the real ones. In this paper, using the ratio method of fixed scale wavelet transformations improved by us, the arrival times for the first arrival phases (such as P and PKIKP) at the teleseismic and far-teleseimic distances were measured. The results are reasonable and reliable based on the analysis and discussion of the reliabilities and errors.

Key words: **Morlet wavelet**; **wavelet transformation ratio**; **first arrival phase**; **first arrival time**; **signal to noise ratio**
CLC number: P315.3^{+}1 **Document code**: A

Introduction

Usually there are abundantly transient high-frequency compositions and weak amplitudes at the onset of a gradually changing signal. Using the method of the fixed scale wavelet transformation ratio, we tried to display and measure the onset time or first arrival time. Unfortunately, the ratio method is lack of the stability. To reduce the noise influence on the ratio, reveal the arrival time information and improve the measurement precision of the arrival time of the gradually changing signals, several schemes have been formed after some synthesized signals and few seismic waves have been studied with that ratio method (LIU *et al*, 2004). However, they have not measured large numbers of real tele-seismograms. The first arrival phases P and PKIKP at tele- and far-tele-seismograms usually rise slowly and gradually, so that it is difficult with eyes to accurately determine their arrival times, and the arrival times measured with the eyes are generally delayed. As well known, a huge amount of data about the arrival times of P and PKIKP are the basis of studying the deep structures of the Earth′s interior, such as body wave tomography and so on. Therefore, it is important to accurately measure the arrival times of P and PKIKP. In this paper, the constrained conditions to the ratio curve of fixed scale Morlet wavelet transformations were studied in more detail, and then were improved and simplified. Subsequently, 50 records of teleseismic and far-teleseimic distances were processed, and so the actual effect of the ratio method and procedure were really further tested.

* **Received date**: 2004-05-13; **revised date**: 2005-04-21; **accepted date**: 2005-04-21.
Foundation item: National Natural Science Foundation of China (40074007).
E-mail of the second author: zhouhl@gacas.ac.cn

1 Simplified and improved method of the fixed scale wavelet transformation ratio

The fixed scale wavelet transformation ratio, noted as FSWTR, was defined as (LIU *et al*, 2004):

$$R(a_2, a_1, b) = \frac{|W(a_2, b)|}{|W(a_1, b)|} \tag{1}$$

where, $W(a, b)$ denote the Morlet complex wavelet transformation of the signal $x(t)$ (ZHENG *et al*, 2001)

$$W(a, b) = \frac{1}{\sqrt{a\sqrt{\pi}}} \int_0^{\infty} \exp\left[\mathrm{i}\omega_{\mathrm{p}} \frac{t-b}{a} - 0.5\left(\frac{t-b}{a} \right)^2 \right] x(t)\mathrm{d}t \tag{2}$$

where, a_1 and a_2 are the different scale factors, and $a_1>a_2$; by experimentation, $a_1=A$ and $a_2=A/2$ are the better choices; $A=\omega_{\mathrm{p}}/\omega_0$, ω_{p} is the modulation frequency and usually taken as 6.0, $\omega_0=2\pi f_0$, f_0 is the main frequency of the signals.

As mentioned above, the ratio method has the defect of instability because of the noises. To reduce the influence of noises, in this paper, the method was further improved and tested by us as follows

1) According to IASPEI1991 model (Kennett, 1991), the theoretical arrival time t_i was computed as the reference point. $|W(A, b)|$ and $|W(A/2, b)|$ were calculated from equation (2), and their first maximum behind t_i was individually written as $\max|W(A, b)|$ and $\max|W(A/2, b)|$.

2) Because of using the module $|W(a, b)|$ of the complex wavelets, the corresponding time t_2 of $\max|W(A, b)|$ is delayed compared with that of $\max|W(A/2, b)|$, and more later than the arrival time of first arrival phase P or PKIKP. Therefore, for measuring the first arrival phases, only the ratio curve $R(A, A/2, b)$ (simplified sign as R below) ahead of t_2 should be considered. To reduce the influence of noises, the values of R from t_1 to t_2 should be calculated, and according to the data conditions, there are two methods to determine t_1.

Method a: If there exist the minimal values at curve $|W(A, b)|$ ahead of t_2, the time corresponding to the minimum closest to $\max|W(A, b)|$ was t_1 (Figure 1a).

Method b: If there do not exist the minimal values at the curve $|W(A, b)|$ ahead of t_2, the time corresponding to $\delta\max|W(A, b)|$ was t_1 (Figure 1b); where δ is an experiential value about 0.01~0.1.

After determining t_1 and t_2, the things only needed to do is to calculate the R from t_1 to t_2, and put zero to other R. So the noises and other phases out of the range from t_1 to t_2 can be avoided.

3) From t_1 to t_2, the arrival time of the first arrival phases t_r corresponding to the first maximal value of R curve can be measured.

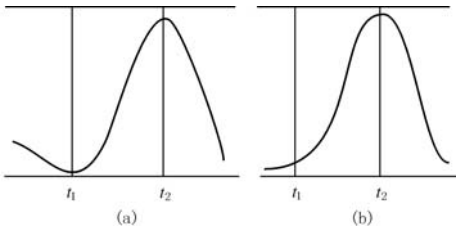

Figure 1 The sketch of method to determine the time range $[t_1, t_2]$
t_2 is the time corresponding to the first maximal value $\max|W(A, b)|$ and t_1 is determined by two methods: (a) The time corresponding to the minimum closest to $\max|W(A, b)|$ is taken as t_1; (b) If there do not exist the minimum, the time corresponding to $\delta\max|W(A, b)|$ is taken as t_1, where δ is about 0.01~0.1

2 Preprocess of the seismograms

Fifty vertical component seismograms recorded at stations with distance larger than 30° were chosen from IRIS Date Management Center for measuring the t_r with our method. These long-period data were firstly preprocessed including removing mean and trend. Table 1 shows the locations, distances and other parameters of the stations.

Table 1 The long-period data and station informations

Station	Time a-mo-d	Epicenter			Depth/km	Distance/(°)
		Location	φ_N/(°)	λ_E/(°)		
MDT	1998-01-27	Fiji Islands	–20.77	–179.18	642.80	167.0
NNA	2000-05-04	Sulawesi, Indonesia	–1.11	–123.57	26.00	155.9
CCM	2000-05-04	Sulawesi, Indonesia	–1.11	–123.57	26.00	131.3
SDV	2000-10-25	Sunda Strait	–6.55	105.63	38.00	175.5
OTAV	2000-10-25	Sunda Strait	–6.55	105.63	38.00	172.5
DWPF	2000-10-25	Sunda Strait	–6.55	105.63	38.00	155.5
FFC	2000-10-25	Sunda Strait	–6.55	105.63	38.00	127.1
ANMO	2000-10-25	Sunda Strait	–6.55	105.63	38.00	139.1
PMSA	2000-08-06	Bonin Islands	28.86	139.56	394.80	141.1
PAYG	2000-08-06	Bonin Islands	28.86	139.56	394.80	125.1
BOSA	2000-08-06	Bonin Islands	28.86	139.56	394.80	123.1
LCO	2000-08-06	Bonin Islands	28.86	139.56	394.80	153.5
CPUP	1996-06-17	Flores Sea	–7.14	–122.59	587.30	146.7
GFA	1996-06-17	Flores Sea	–7.14	–122.59	587.30	113.4
PTGA	1996-06-17	Flores Sea	–7.14	–122.59	587.30	171.8
BOSA	2001-01-10	Kodiak Island	57.09	–153.62	33.00	151.5
SUR	2001-01-10	Kodiak Island	57.09	–153.62	33.00	155.0
SJG	2003-05-26	Halmahera, Indonesia	2.35	128.86	31.00	154.8
PAYG	2003-05-26	Halmahera, Indonesia	2.35	128.86	31.00	140.8
CCM	2003-05-26	Halmahera, Indonesia	2.35	128.86	31.00	125.1
LTX	2003-05-26	Halmahera, Indonesia	2.35	128.86	31.00	120.7
PMSA	2003-05-26	Halmahera, Indonesia	2.35	128.86	31.00	117.0
LCO	2002-03-03	Hindu kush, Afghanistan	36.50	70.48	225.60	146.5
LVC	2002-03-03	Hindu kush, Afghanistan	36.50	70.48	225.60	142.3
PMSA	2002-03-03	Hindu kush, Afghanistan	36.50	70.48	225.60	141.0
SBA	2002-03-03	Hindu kush, Afghanistan	36.50	70.48	225.60	126.7
LCO	2002-11-17	Northwest of Kuril Islands	47.82	146.21	459.10	145.9
LVC	2002-11-17	Northwest of Kuril Islands	47.82	146.21	459.10	142.4
NNA	2002-11-17	Northwest of Kuril Islands	47.82	146.21	459.10	129.4
PLCA	2002-03-05	Mindanao Philippine Islands	6.03	124.25	31.00	143.0
PAYG	2002-03-05	Mindanao Philippine Islands	6.03	124.25	31.00	145.1
PLAL	2002-03-05	Mindanao Philippine Islands	6.03	124.25	31.00	129.1
WDD	2000-02-25	Vanuatu Islands	–19.53	173.82	33.00	155.6
CII	2000-02-25	Vanuatu Islands	–19.53	173.82	33.00	151.9
RCBR	2002-03-26	Southwestern Ryukyu Islands	23.35	–124.09	33.00	154.0
EFI	2002-03-26	Southwestern Ryukyu Islands	23.35	–124.09	33.00	151.7
SJG	2002-03-26	Southwestern Ryukyu Islands	23.35	–124.09	33.00	137.6
BNI	2002-01-02	Vanuatu Islands	17.60	–167.86	21.00	148.4
ASCN	2002-01-02	Vanuatu Islands	17.60	–167.86	21.00	154.5
VSL	2002-01-02	Vanuatu Islands	17.60	–167.86	21.00	151.3
RUE	2002-01-02	Vanuatu Islands	17.60	–167.86	21.00	139.7
ANMO	2002-06-27	Sunda Strait	–6.96	104.18	11.00	140.4
RCBR	2002-06-27	Sunda Strait	–6.96	104.18	11.00	138.2
FFC	2002-06-27	Sunda Strait	–6.96	104.18	11.00	128.0
CCM	2001-06-23	Near coast of Peru	–16.14	–73.31	33.00	56.5
ANMO	2001-06-23	Near coast of Peru	–16.14	–73.31	33.00	59.8
PMSA	2001-06-23	Near coast of Peru	–16.14	–73.31	33.00	49.0
MPM	2001-06-23	Near coast of Peru	–16.14	–73.31	33.00	66.6
MLAC	2001-06-23	Near coast of Peru	–16.14	–73.31	33.00	68.5
DJJ	2001-06-23	Near coast of Peru	–16.14	–73.31	33.00	65.9

3 Cuting the seismic waveforms

When processing the teleseismic phase P, the length T_w of the time window is often taken from 30 s to 65 s, *i.e*. cutting the waveform at the 10~25 s ahead of the arrival time t_0 of P measured by eyes, and 20~40 s behind it. When processing the far-teleseismic phase PKIKP, T_w is from 45 s to 85 s, *i.e*. cutting the waveform at 15~25 s ahead of the arrival time t_0 of PKIKP measured by eyes, and 30~60 s behind it. When cutting the waveform data, if the period of the P or PKIKP is obvious, T_w should exceed one whole period at least, otherwise T_w should be taken as the maximal value mentioned above.

The time window should farthest only include the concerned phase in order to limit the spreading range of the frequencies of the signals, and improve the precision of main frequency measurement from the graph of time-frequency analysis. If two phases (when another phase is very close to P or PKIKP) are into the time window, we can measure their frequencies, and set the larger one as main frequency f_0 into equation (1).

When the main frequency f_0 is very small (some values are less than 0.1 Hz), so the T_w should be extended. But the overlong length will lead to include other phases. Therefore, based on the numerical experimentations and data confirmations, the projects of cutting data considered above are reserved in the paper, but the values of $2f_0$ will be used to calculate the wavelet transformation when f_0 less than 0.125 Hz.

4 Time-frequency analysis

We applied time-frequency analysis to the cut data, and accurately measured the main frequency f_0. From equation (1), it can be seen the accurate f_0 is the key to calculate ratio value R. We used Choi-Williams method to make time-frequency analysis (Cohen, 1994).

5 Arrival time measurements of P and PKIKP

After data preprocessing, waveforms cut and time-frequency analysis, according to equation (1) and the improved method mentioned above, the data of arrival time t_r were obtained. The whole measuring process is illustrated with some examples. The station ANMO recorded an earthquake (with original time of 2001-06-23) with distance Δ=59.8° and first arrival phase P. It can be seen by the cut waveform (Figure 2-1a and 2-2a), the noise is weak and the onset of P is slow but distinct. The P onset time t_0 observed by eyes and t_i predicted from IASPEI1991 is 32 s and 30 s relative to the beginning of the data window, respectively. The time-frequency analysis of waveform shows three obvious frequency components and their maximum 0.13 Hz is considered as the main frequency f_0, then $A=\omega_p/\omega_0$=7.345 6. The calculated $|W(A/2, b)|$, $|W(A, b)|$ and $R(A, A/2, b)$ is denoted in Figure 2-2b, 2-2c and 2-2d, respectively. The end time t_2 of $R(A, A/2, b)$ is determined by the first maximal peak value max$|W(A, b)|$ and the starting time t_1 is obtained from the 0.07 max$|W(A, b)|$. The P arrival time t_r measured at the maximum of $R(A, A/2, b)$ in the time segment $[t_1, t_2]$ is 32 s.

The t_r is the same as t_0 by eyes, and $\Delta t=t_0-t_r=0$. As mentioned above, because of the weak noises in this waveform (high R_{sn} of 47 dB) and the slow but distinct onset, the two measurements results are the same.

Figure 3-1a and 3-2a are the seismograms of event 2003-05-26 recorded at station PAYG with distance Δ=140.8°. Because of the low R_{sn}=8 dB, it is difficult to measure the arrival time by

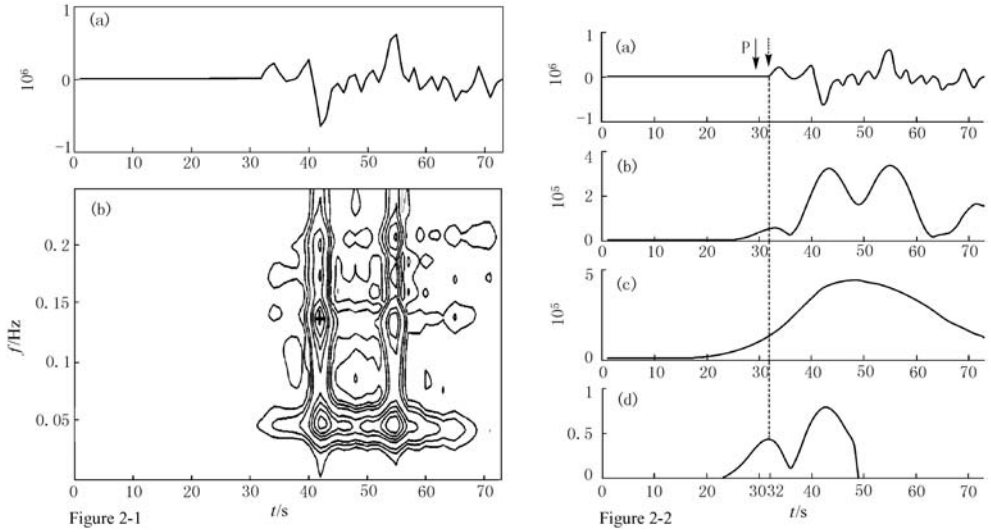

Figure 2 2001-06-23 earthquake recorded by ANMO station (Δ=59.8°) and measurement of the first arrival phase P

(2-1) Waveforms and time-frequency analysis: (a) The cut waveform; (b) Time-frequency analysis, the main frequency is the vertical coordinate of the maximal energy (solid cross) 0.13 Hz; (2-2) waveforms and measurement of the arrival time of P phase: (a) The cut waveform (same as 2-1a), the solid arrow marks the predicted arrival time t_i from IASPEI1991, and the dashed arrow marks the arrival time t_0 measured by eyes; (b) The module of the complex Morlet wavelet transformation of $A/2$ scale: $|W(A/2, b)|$; (c) The module of the complex Morlet wavelet transformation of A scale: $|W(A, b)|$; (d) The ratio of the wavelet transformation: $R(A, A/2, b)$, the time segment $[t_1, t_2]$ was determined by the method b mentioned above, the long dashed line marks the arrival time measured by this method, and the time is t_r

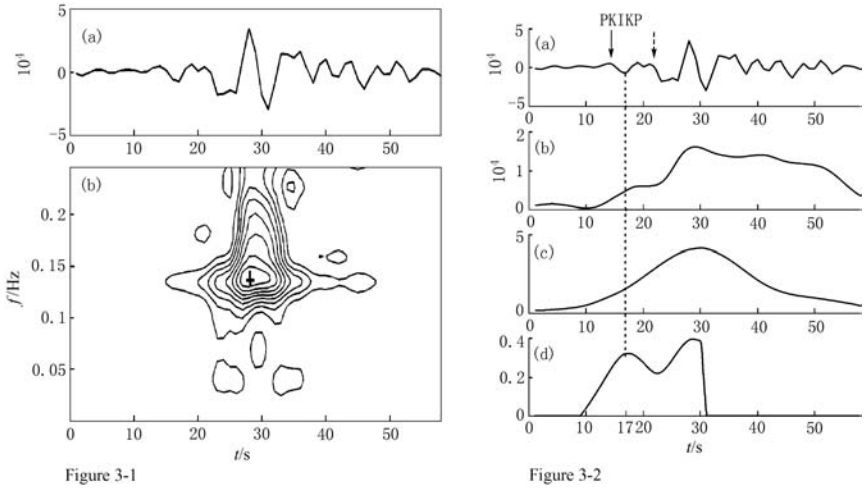

Figure 3 2003-05-26 earthquake (Δ=140.8°) recorded by PAYG station and measurement of the first arrival phase PKIKP

(3-1) Waveforms and time-frequency analysis: (a) The cut waveform; (b) Time-frequency analysis, the main frequency is the vertical coordinate of the maximal energy (solid cross) 0.14 Hz; (3-2) Waveforms and measurement of the arrival time of PKIKP phase: (a) The cut waveform (same as 3-1a), the solid arrow marks the predicted arrival time t_i from IASPEI91, and the dash arrow marks the arrival time t_0 measured by eyes; (b) The module of the complex Morlet wavelet transformation of $A/2$ scale: $|W(A/2, b)|$; (c) The module of the complex Morlet wavelet transformation of A scale: $|W(A, b)|$; (d) The ratio of the wavelet transformation: $R(A, A/2, b)$, the time segment $[t_1, t_2]$ was determined by the method b mentioned above, the long dashed line marks the arrival time measured by this method, and the time is t_r

eyes, and t_0 is 22 s approximately. The waveform was cut according to the predicted time t_i=14 s. By time-frequency analysis (Figure 3-1b), the main frequency f_0=0.14 Hz and so A=6.8209. The calculated $|W(A/2, b)|$, $|W(A, b)|$ and $R(A, A/2, b)$ is denoted in Figure 3-2b, 3-2c and 3-2d, individually. The end time t_2 of $R(A, A/2, b)$ is determined by the first maximal peak value $\max|W(A, b|$ and the starting time t_1 is obtained from the 0.1 $\max|W(A, b)|$. The P arrival time t_r is 17 s measured at the maximum of $R(A, A/2, b)$ in the time segment $[t_1, t_2]$, and the Δt is equal to 5 s.

Figure 4-1a and 4-2a are the seismograms of event 1998-01-27 recorded at station MDT with distance Δ=167.0°. Because of low R_{sn} of 2 dB, it is also difficult to measure the arrival time by eyes and t_0 is 39 s approximately. The waveform was cut according to the predicted time t_i=34 s. By time-frequency analysis (Figure 4-1b), the main frequency f_0=0.14 Hz, so A=6.3662. The calculated $|W(A/2, b)|$, $|W(A, b)|$ and $R(A, A/2, b)$ is shown in Figure 4-2b, 4-2c and 4-2d, individually. The t_2 of time segment $[t_1, t_2]$ is obtained as same as the above, and the t_1 is got from the time corresponding to the minimal value closest left to $\max|W(A, b)|$. The P arrival time t_r is 39 s measured at the maximum of $R(A, A/2, b)$ in the time segment $[t_1, t_2]$, then the Δt is zero. This result seems mean that the departure between measurements by eyes and that by this method is small when the P onset pulse is strong, even if the background noises are high.

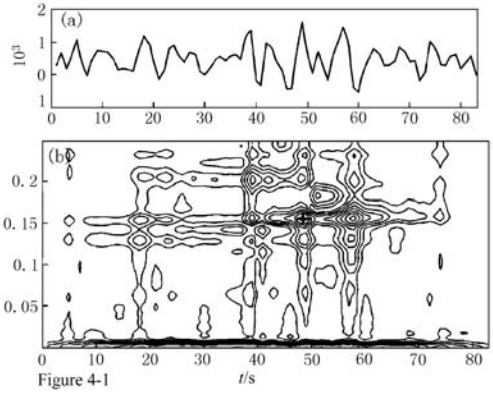

Figure 4-1

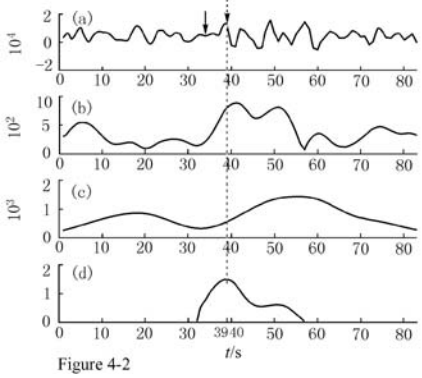

Figure 4-2

Figure 4 1998-01-27 earthquake recorded by MDT station (Δ=167.0°) and measurement of the first arrival phase PKIKP

(4-1) Waveforms and time-frequency analysis: (a) The cut waveform; (b) Time-frequency analysis, the main frequency is the vertical coordinate corresponding to the maximal energy(solid cross) 0.15 Hz; (4-2) Waveforms and measurement of the arrival time of PKIKP phase: (a) The cut waveform (same as 4-1a), the solid arrow marks the predicted arrival time t_i from IASPEI1991, and the dashed arrow marks the arrival time t_0 measured by eyes; (b) The module of the complex Morlet wavelet transformation of $A/2$ scale: $|W(A/2, b)|$; (c) The module of the complex Morlet wavelet transformation of A scale: $|W(A, b)|$; (d) The ratio of the wavelet transformation: $R(A, A/2, b)$, the time segment $[t_1, t_2]$ was determined by the method a as the mentioned above, the long dashed line marks the arrival time measured by this method, and the time is t_r

6 Analysis of the results and errors

6.1 Results analysis

We obtained the arrival time t_r of the first arrival phases P or PKIKP by the FSWTR method, t_0 by eyes, the arrival time difference Δt ($\Delta t=t_0-t_r$), theoretical arrival time t_i on the IASPEI1991 model and the signal to noise ratio (R_{sn}) of the original data. From Table 2 and Figure 5, it can be seen that t_0 is mostly delayed and a few equal to t_r. In the practice, It is noticed that there exist the large errors when researchers identify and measure the phases P and PKIKP because their onsets

are generally weak and gradually changing, measured time by eyes is corresponding to the enhancement of the obvious amplitude which is not the starting time of the phase and later than it. This phenomenon was also quantitatively explained and validated by the results of the 50 data dealt with by us. From Figure 6 we can see that the most Δt values are smaller than 7 s, and within them Δt=0 has highest appearance frequency. The result that t_r is the same as t_0 when the onset of P or PKIKP is distinct indicates the reliability of our method. When the onset of P or PKIKP is very weak and gradually changing or interfered by strong noises, the result that t_r is smaller than t_0 shows the rationality of our method.

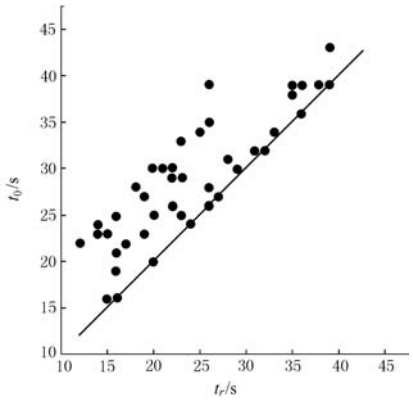

Figure 5 Analytical comparision of t_r with t_0

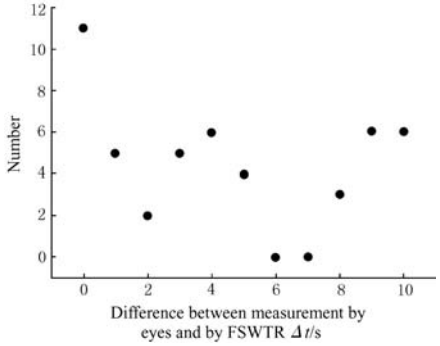

Figure 6 Difference between measurement by eyes and by FSWTR and appearance frequency

6.2 Errors analysis

Two parts contribute to the measured errors. Firstly noise results in the errors at the main frequency analysis, and finally leads to the errors at the measured results. Secondly the errors come from the instability of FSWTR method caused by noise. The distribution characteristic of R_{sn} values by analyzing the 50 data is shown in Figure 7. Based on the real R_{sn} of the original data, synthesized signals with various R_{sn} were formed, and the mathematics model of the signals can be written as:

$$S(t) = t\exp(-0.05t)\cos(10\pi t)u(t-1) + n(t) \tag{3}$$

where $u(t-1)$ is unit step function, $n(t)$ denotes the random noise formed according to the real R_{sn}.

By the numerical experimentations, the result influenced by the above two parts were considered and measured as follows.

1) Influence of noise on main frequency measurement. When R_{sn} <4 dB, the errors of f_0 is ±0.01 Hz, according to equations (1) and (2), the errors of t_r measured by the method of FSWTR is δt_1=±1 s; when R_{sn} ≥4 dB, the measured error of f_0 is almost zero, and no influence on the measurement of t_r.

2) Influence of noise on the method stability. When R_{sn} <15 dB, the error of t_r is δt_2=±2 s; when 15 dB≤ R_{sn} ≤25 dB, δt_2=±1 s; when R_{sn} >25 dB, the error is almost zero.

Simultaneously considering the two parts of influences，the maximal error δt of the measurement is the summation of two parts, so when R_{sn}<4 dB, δt=±3 s; when 4 dB≤ R_{sn} <15 dB, δt=±2 s; when 15 dB≤ R_{sn} ≤25 dB, δt=±1 s; when R_{sn} >25 dB δt≈0.

Table 2 The results of measurement of the arrival time of the phases (P and PKIKP) using FSWTR

Station	Epicentral distance /(°)	Phase	*f*/Hz	Arrival time relative to the begin of the time window/s				R_{sn} /dB	Order	First arrvial phase onset of the original data
				t_o	t_i	t_r	Δt			
PMSA	49.0	P	0.05	21	17	16	5	37	45	Weak noise, very slow onset
CCM	56.5	P	0.14	24	20	24	0	53	50	Weak noise, slow onset
ANMO	59.8	P	0.13	32	30	32	0	47	49	Weak noise, slow onset
DJJ	65.9	P	0.13	16	13	16	0	30	42	Weak noise, slow onset
MPM	66.6	P	0.10	30	27	29	1	42	47	Weak noise, slow onset
MLAC	68.5	P	0.09	20	17	20	0	42	48	Weak noise, slow onset
GFA	113.4	PKIKP	0.09	30	25	20	10	31	40	Weak noise, very slow onset
PMSA	117.0	PKIKP	0.14	19	15	16	3	1	1	Strong noise, slow onset
LTX	120.7	PKIKP	0.18	39	34	26	3	15	18	Strong noise, slow onset
BOSA	123.1	PKIKP	0.19	36	33	36	0	11	12	Strong noise, slow onset
PAYG	125.1	PKIKP	0.20	39	37	35	4	13	14	Strong noise, slow onset
CCM	125.1	PKIKP	0.18	28	26	18	10	18	25	Strong noise, very slow onset
SBA	126.7	PKIKP	0.22	23	20	15	8	14	16	Strong noise, very slow onset
FFC	127.1	PKIKP	0.22	33	32	23	10	10	10	Strong noise, very slow onset
FFC	128.0	PKIKP	0.18	34	32	25	9	20	30	Strong noise, very slow onset
PLAL	129.1	PKIKP	0.06	26	24	22	4	14	17	Strong noise, slow onset
NNA	129.4	PKIKP	0.18	23	21	14	9	29	41	Weak noise, very slow onset
CCM	131.3	PKIKP	0.12	38	33	35	3	23	33	Weak noise, slow onset
SJG	137.6	PKIKP	0.20	23	20	19	4	11	13	Strong noise, slow onset
RCBR	138.2	PKIKP	0.08	27	20	27	0	17	23	Strong noise, slow onset
ANMO	139.1	PKIKP	0.13	39	39	36	3	15	19	Strong noise, slow onset
RUE	139.7	PKIKP	0.15	28	21	26	2	19	27	Weak noise, slow onset
ANMO	140.4	PKIKP	0.09	26	20	26	0	26	37	Weak noise, slow onset
PAYG	140.8	PKIKP	0.14	22	14	17	5	8	8	Strong noise, very slow onset
PMSA	141.0	PKIKP	0.13	25	34	20	5	10	11	Strong noise, very slow onset
PMSA	141.1	PKIKP	0.04	39	43	38	1	6	6	Strong noise, slow onset
LVC	142.3	PKIKP	0.13	32	30	31	1	15	20	Strong noise, slow onset
LVC	142.4	PKIKP	0.18	30	31	22	8	24	34	Weak noise, very slow onset
PLCA	143.0	PKIKP	0.05	30	28	21	9	19	28	Strong noise, very slow onset
PAYG	145.1	PKIKP	0.06	24	20	24	0	18	26	Strong noise, slow onset
LCO	145.9	PKIKP	0.16	22	21	12	10	22	32	Weak noise, very slow onset
LCO	146.5	PKIKP	0.09	22	26	17	5	16	22	Strong noise, very slow onset
CPUP	146.7	PKIKP	0.09	29	20	22	7	31	43	Weak noise, very slow onset
BNI	148.4	PKIKP	0.05	24	20	14	10	24	35	Weak noise, very slow onset
VSL	151.3	PKIKP	0.15	35	22	26	9	26	38	Weak noise, very slow onset
BOSA	151.5	PKIKP	0.15	25	20	16	9	6	7	Strong noise, very slow onset
EFI	151.7	PKIKP	0.15	27	20	19	8	9	9	Strong noise, very slow onset
CII	151.9	PKIKP	0.14	34	24	33	1	19	29	Strong noise, slow onset
LCO	153.5	PKIKP	0.15	24	16	14	10	13	15	Strong noise, very slow onset
RCBR	154.0	PKIKP	0.16	31	24	28	3	3	4	Strong noise, slow onset
ASCN	154.5	PKIKP	0.14	30	25	21	9	20	31	Weak noise, very slow onset
SJG	154.8	PKIKP	0.13	24	22	24	0	17	24	Strong noise, slow onset
SUR	154.9	PKIKP	0.14	16	17	15	1	4	5	Strong noise, slow onset
DWPF	155.5	PKIKP	0.10	29	25	23	6	2	2	Strong noise, very slow onset
WDD	155.6	PKIKP	0.14	16	14	16	0	15	21	Strong noise, slow onset
NNA	155.9	PKIKP	0.09	43	42	39	4	32	44	Weak noise, slow onset
MDT	167.0	PKIKP	0.15	39	34	39	0	2	3	Weak noise, slow onset
PTGA	171.8	PKIKP	0.09	25	20	23	2	37	46	Weak noise, slow onset
OTAV	172.5	PKIKP	0.12	23	20	19	4	25	36	Weak noise, slow onset
SDV	175.5	PKIKP	0.12	26	23	22	4	27	39	Weak noise, slow onset

Note: t_0: Arrival time measured by eyes; t_i: Theoretical arrival time for IASPEI1991model; t_r: Arriral time measured by FSWTR; $\Delta t=t_0-t_r$; Order: Number ranked the origin data according to the R_{sn} from weak to strong.

7 Discussion and conclusions

1) The FSWTR method improved by us is simple and convenient on recognizing and measuring the arrival time of the weak and slow onset seismic phases, and the results are reasonable and reliable after the arrival time of the teleseismic and far-teleseismic phase (P and PKIKP) were measured and studied.

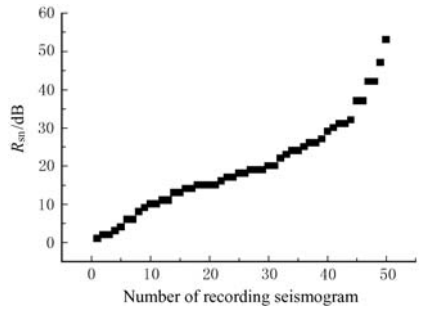

Figure 7 Distribution of the R_{sn} of the data

2) Because the sample rate of the long period data is one point per second, it limits the measurement precision of t_r. Time-frequency analysis is important and the accurate value of the main frequency ensure the preciseness of the FSWTR method. The real data treatment shows the maximal frequency should be selected as the main frequency when the energies of several frequencies are prominent. If the noise is too strong to determine the main frequency, the method is not feasible to be used to measure the arrival time.

3) We will deal with more data in relation to other researches, and further test and perfect the FSWTR method.

Acknowledgments: We are grateful for helpful discussions with MA Yan-lu and LIU Xi-qiang and assistances for using seismic wave analytical softwares. We also deeply thank IRIS for providing seismic waveform data and Sandia National Laboratory for Matseis software.

References

Cohen L. 1994. *Time Frequency Analysis*: *Theory and Applications* [M]. New York: Prentice Hall PTR, 168.

Kennett B L N. 1991. *IASPEI* 1991 *Seismological Tables* [M]. Canberra: Bibliotech, 1~167.

LIU Xi-qiang, ZHOU Hui-lan, HE Xiao-bo *et al*. 2004. Complex wavelets analysis and application in recognizing the gradually change style seismic phases [A]. In: :CHEN Yuan-tai, TENG Ji-wen, KAN Rong-ju *et al* ed. *The Research Progress in the Chinese Mainland Seismology and the Earth Interior Physics– Celebrating Academician Zeng Rongsheng's 80th Anniversary* [C]. Beijing: Seismological Press, 752~760 (in Chinese).

ZHENG Zhi-zhen, SHEN Pin, YANG Xuan-hui *et al*. 2001. *Wavelet Transformation and the Application of MATLAB Tool* [M]. Beijing: Seismological Press, 50~120 (in Chinese).